3D-printed multi-functional foamed concrete building components: Material properties, component design, and 3D printing application

Developments in the Built Environment 20 (2024) 100483

Contents lists available at ScienceDirect

Developments in the Built Environment

journal homepage: www.sciencedirect.com/journal/developments-in-the-built-environment

3D-printed multi-functional foamed concrete building components: Material properties, component design, and 3D printing application

Silvia Parmigiani [a], Devid Falliano [a,*], Sandro Moro [b], Giuseppe Andrea Ferro [a], Luciana Restuccia [a]

[a] Department of Structural, Building and Geotechnical Engineering, Politecnico di Torino, Italy
[b] Master Builders Solutions Italia Spa, Treviso, Italy

ARTICLE INFO

Keywords:
3D concrete printing
Ultra-lightweight foamed concrete
Thermal conductivity
Energy-efficient building components
Design and robotic application

ABSTRACT

The use of multi-density foamed concretes (FCs) to produce multi-functional building components by 3D Concrete Printing (3DCP) is investigated. The use of medium-density 3D-printed foamed concrete (3DPFC_800), primarily serving a load-bearing role, and ultra-lightweight foamed concrete (ULFC_300), as thermal insulation material poured in the voids defined by the former, is proposed. This enables meeting diverse performance requirements within a single cementitious matrix, eliminating the need for multiple materials. The main properties of the proposed mixes are investigated. The compressive strength and thermal conductivity are equal to 7.04 MPa and 0.205 W/mK, and 1.43 MPa and 0.072 W/mK for 3DPFC_800 and ULFC_300, respectively. A successful 2D-printing test validates the suitability of 3DPFC_800 for 3DCP, and a robotic arm is employed for 3DCP tests. The proposed application allows for further knowledge on the use of FC in 3DCP and the identification of some issues and challenges that still need to be addressed.

1. Introduction

Over the last 30 years, the use of lightweight concrete has become increasingly widespread throughout the world. Compared to traditional concrete, lightweight concrete offers enhanced sustainability, weight reduction, multifunctionality, and versatility while maintaining high technical performance. Among lightweight concretes, Foamed Concrete (FC) stands out as a cellular material that can be easily produced using simple methods such as pre-formed foaming method or mixing-foaming method. These processes could be executed on-site using common materials like binder, water, foaming agents (synthetic or protein-based), fine aggregates like sand (typically for densities above 800 kg/m^3), additives and other possible additions such as fibers. With densities ranging from 90 kg/m^3 (Falliano et al., 2022) to 1800 kg/m^3 depending on mix design, FC proves highly adaptable for both structural and non-structural applications. Furthermore, the broad range of densities makes it possible, depending on the specific case, to tailor the mix design to obtain cementitious mixes with the desired properties. Overall, foamed concrete exhibits adequate mechanical strength and durability (especially at higher densities), excellent thermal insulation and fire resistance (particularly at lower densities), all while offering cost and environmental advantages over standard concrete.

To date, FC has undergone extensive study to deepen understanding of its properties and optimize mix designs across different densities. In this regard, some researchers (Fu et al., 2020), (Chica and Alzate, 2019), (Ramamurthy et al., 2009), classified numerous studies in the literature, providing a comprehensive overview of FC characteristics. Other authors focused on some specific aspects: the effects of foaming agents of different nature on the characteristics and performance of foamed concrete (Panesar, 2013), (Hashim and Tantray, 2021), (Falliano et al., 2021); fresh-state instability (Jones et al., 2016); hardened-state properties at different densities, such as compressive strength, microstructural characteristics, thermal conductivity (Mydin, 2011), durability, geometric conformity. Others studied some variables that might influence the aforementioned properties, such as foam generation and foam properties (Hashim and Tantray, 2021), curing conditions, cement type, foaming agent and target dry density (Falliano et al., 2018), porosity and void size (Mydin, 2022a), (Nambiar and Ramamurthy, 2007), filler type (Nambiar and Ramamurthy, 2006), addition of fibers (Raj et al., 2020), (Mydin, 2022b), and other kinds of additions derived from wastes, with a pozzolanic and/or filler function, such as fly ash, furnace slag and mineral powder (Song et al., 2021), or fly ash and quarry dust

* Corresponding author. Corso Duca Degli Abruzzi, 24, Politecnico di Torino, Italy.
E-mail address: devid.falliano@polito.it (D. Falliano).

https://doi.org/10.1016/j.dibe.2024.100483
Received 19 February 2024; Received in revised form 7 May 2024; Accepted 13 June 2024
Available online 14 June 2024

(Gopalakrishnan et al., 2020). Finally, other authors (Falliano et al., 2022), (Jones et al., 2017), (Jiang et al., 2016), focused on the characteristics and performance of ultra-lightweight foamed concrete, i.e., characterized by a dry density lower than 300 kg/m^3 and mainly intended for use as thermal insulation.

Nevertheless, although studies on foamed concrete have been numerous, providing a comprehensive understanding of this material, few studies have explored the exciting field of its application in 3D Concrete Printing.

Among Digital Fabrication with Concrete (DFC) processes, 3D Concrete Printing (3DCP) stands out as the most promising and extensively studied automated construction system. Integrating FC into 3DCP holds the potential to combine the benefits of FC with those of automated processes, thereby broadening the application scope of 3DCP technology. The advantages of 3DCP include complete design freedom and customization (du Plessis et al., 2021), (Zhang et al., 2018), (Lim et al., 2012), scalability from individual components to entire buildings (Lim et al., 2012), (Rollakanti and Prasad, 2022), (Xiao et al., 2021), (Wu et al., 2016), (Gosselin et al., 2016), (Bos et al., 2016), and potential cost and environmental savings compared to traditional construction practices. The latter goal can be achieved thanks to the elimination of traditional formwork, by adopting optimized design strategies, such as topological optimization of structural sections and functional hybridization, and by avoiding any kind of waste (De et al., 2018). However, some limitations and challenges still need to be addressed to effectively apply 3DCP technology in the daily construction practice. These aspects are treated by Buswell et al. (2018) and by De Schutter et al. (De et al., 2018) from a technical, economic, and environmental perspective, while Khan et al. (2020) reported the state-of-art and state-of-practice of 3DCP, and the latest advances in equipment, materials, and computer modeling.

To date, 3DCP is primarily applied to mortars or normal-weight concrete, despite recent literature highlighting the potential benefits of extending its application to FC (Rudziewicz et al., 2023), (Falliano et al., 2019a), (Markin et al., 2021). Among these, Rudziewicz et al. (2023) underscored the advantages of enhanced productivity and reduced construction costs, as well as the alignment of building practices with circular economy principles. This alignment is facilitated by the elimination of additional insulating layers, thereby minimizing the need for materials other than concrete. Moreover, it streamlines end-of-life recycling processes and promotes the reuse of construction waste, thereby conserving nonrenewable natural resources and reducing CO2 emissions. The potential applications are extensive, including structural applications (Cho et al., 2019), load-bearing and insulating elements for multi-story buildings (Markin et al., 2019a), suspended ceilings (Falliano et al., 2019b), wall elements without insulation layers in hot climates (Markin et al., 2021), foamed facade elements (Cho et al., 2021), energy efficiency interventions on existing walls to achieve highly insulating, easily recyclable, and customizable facades (Lublasser et al., 2018), multi-density and multi-property elements combining lightness and high strength (Geng et al., 2022), walls with optimized cavities based on thermal performance (Marais et al., 2021), multi-density elements produced through variable-density FC printing (Adaptive foam concrete) (Schmid et al., 2022), multi-layer insulating panels (Falliano et al., 2019a), and lightweight thermal-insulating mortar (Gao et al., 2023).

Nevertheless, the field of 3D-Printable Foamed Concrete (3DPFC), as previously mentioned, remains largely unexplored, with research still in its nascent stages. Some authors have focused on material design (Markin et al., 2019a), while others have addressed possible mixing methods (Markin et al., 2019b), (Zhang and Sanjayan, 2024), foam stability in the case of use of pre-formed foaming method (Cho et al., 2022), and the effects of foaming agents of different natures (synthetic or protein-based) on material properties (Markin et al., 2019b), (Boddepalli et al., 2023).

However, the main challenges are related to fresh-state properties. In particular, one of the most significant, and thus extensively studied in existing literature, is related to the typically low yield stress values characterizing FC in its fresh state. In fact, the presence of air bubbles in the fresh cementitious mixture leads to a notable reduction in yield stress values, enhancing material fluidity and pumpability but compromising printability and buildability. Nevertheless, the latter, which, as already mentioned, is ensured by an adequate yield stress value, is a fundamental property for the printability of fresh cementitious pastes (Muthukrishnan et al., 2021). Indeed, to ensure suitable printability, materials usually need to exhibit good thixotropy: low dynamic yield stress promotes pumpability and extrudability, whereas high static yield stress and viscosity recovery characteristics promote good buildability (Chen et al., 2020), (Rahul et al., 2019), (Tay et al., 2019). Since the porosity of the material increases as the density decreases (Kearsley and Wainwright, 2002), obtaining 3DPFC is more arduous as the material's density is lower. This is evident since there are very few examples in the relevant literature of printable foamed concrete with densities lower than 1000 kg/m^3. Only two studies have referenced 3D-printing experiments involving 3DPFC with a density below 600 kg/m^3 (Lublasser et al., 2018), (Schmid et al., 2022).

In the existing literature, various authors have explored diverse methods to improve fresh-state properties of FC for potential 3DCP applications. These methods include the utilization of hydroxypropyl methylcellulose (Gao et al., 2023), possibly combined with silica fume (Liu et al., 2021), (Liu et al., 2022a), (Liu et al., 2023), silica fume or aluminosilicate (Markin et al., 2021), (Markin et al., 2020), sulphoaluminate cement (Liu et al., 2022b), nano-silica (Cho et al., 2019), (Cho et al., 2020), and the employment of a Viscosity Enhancing Agent (VEA) (Falliano et al., 2020a). The objective of these approaches is to enhance static yield stress, dynamic yield stress, and plastic viscosity, thereby ensuring the printability and buildability of FC. Some examples of 3D-printing applications are depicted in (Cho et al., 2021), (Marais et al., 2021), (Schmid et al., 2022), (Zhang and Sanjayan, 2024), (Cho et al., 2022).

In the present study, as detailed in the following section (see **2**), a potential application of FC in 3DCP processes is proposed through the introduction of a Viscosity Enhancing Agent (VEA), which has been employed in previous studies by the authors and enables printability of FC (Falliano et al., 2020a). Specifically, the study presents a design methodology for developing highly optimized multifunctional building components with customized mechanical and thermal properties. These components integrate 3D-printable foamed concrete with a targeted dry density of 800 kg/m^3 (3DPFC_800), primarily serving a load-bearing role, and ultra-lightweight foamed concrete with a targeted dry density of 300 kg/m^3 (ULFC_300), primarily serving as thermal insulation filling for the voids defined by the former.

After defining key properties, such as 2D-printability and drying shrinkage for 3DPFC_800, and compressive strength and thermal conductivity for both 3DPFC_800 and ULFC_300, the gathered data was utilized to design two examples of multifunctional building components, aligning with the desired thermal performance objectives. Subsequently, a practical application of 3DCP utilizing 3DPFC_800 was executed with the assistance of a robotic arm.

2. Research aim

The primary goal of the present preliminary study is to introduce a design methodology that exploits the potential synergy among various densities of a singular cementitious material, specifically FC, to meet multiple customizable performance requirements simultaneously. The approach aims to create building components with tailored mechanical properties and thermal characteristics, precisely outlined as objectives customizable to each specific case.

The study also explores the feasibility of producing at least a portion of these components using 3DCP processes, as the combination of FC and 3DCP would offer advantages such as improved thermal performance

and topological optimization. For this type of application, the traditional FC mix design is modified by adding a Viscosity Enhancing Agent (VEA) to ensure that the material possesses the rheological properties necessary for effective utilization in such processes. This additional challenge provides an opportunity to delve deeper into the application of FC in 3DCP processes, a cutting-edge research topic that is currently facing its initial challenges.

The proposed design approach is tailored to produce lightweight infill walls with self-supporting properties, while meeting specific mechanical strength and thermal conductivity objectives and local regulations. This is achieved by utilizing a singular material with customizable densities, forming multifunctional building components.

The utilization of these elements for infill construction would allow for the realization of customized, multifunctional walls, eliminating the need for stratigraphy with materials of different nature, such as the need for synthetic thermal insulation materials. This not only would simplify the construction and decommissioning phases but would provide environmental and cost-saving benefits as well.

Furthermore, the research envisions the development of prefabricated components in a factory or on-site once digital fabrication transitions are achieved. In this regard, digital fabrication of this type of elements for building envelopes would be easier to achieve, as the age-old question of implementing structural reinforcements would not arise (Asprone et al., 2018). In addition, the multifunctional components could be used in new constructions or to enhance existing buildings' energy efficiency while providing aesthetic façade renovation, as, for instance, proposed on a theoretical level by Lublasser et al. (2018).

In this study, the potential application of the proposed design methodology is illustrated by developing two sample components ideal for the construction of lightweight walls, whether realized off-site or on-site. These components are specifically designed for energy-efficient interventions in existing buildings, as will be clarified afterwards (see **4.2**). For the design of the sample components, the integrated use of 3D-printable foamed concrete with a target dry density of 800 kg/m^3 (3DPFC_800), primarily serving the structural function, and ultra-lightweight foamed concrete with a target dry density of 300 kg/m^3 (ULFC_300), primarily serving as filling for the voids defined by the former, is investigated.

After defining some key properties of the two materials, the design of the components proceeded based on thermal performance. In fact, the component stratigraphy was defined to meet regulatory requirements for thermal performance, which were evaluated by means of UNI EN ISO 13786.

Finally, an application of 3DCP using 3DPFC_800 was carried out. This application allowed to define the current level of feasibility in terms of printability of 3DPFC_800 (according to the methods employed in this study), identifying any open problems and challenges that still need to be solved, trying to assess their possible causes, and proposing possible solutions.

It is important to note that the investigated application is just one of the possible uses of the proposed design method, and the two designed components are examples of what can be achieved with the results obtained from the performance evaluation of the two considered materials.

In the end, the latest innovative aspect of this research involves the utilization of the mixing-foaming method for the production of 3DPFC_800. Unlike the typically used pre-formed foaming method, this alternative method involves incorporating air bubbles within the cementitious matrix during turbulent mixing at a very high speed (mixing intensity equal to 3000 rpm), without the need for pre-formed foam. In this case, the mixing time becomes crucial; a longer mixing time is associated with a lower density due to the greater number of air bubbles formed and incorporated within the mixture. Experimentations have highlighted the effectiveness and repeatability of the method: mixing the same amount of material for the same duration consistently results in the same final density of the mixture. Although, to date, all studies on 3DPFC have employed the pre-formed foaming method, and some authors (Markin et al., 2019a), (Markin et al., 2019b), have deemed this method unsuitable for producing 3DPFC using a protein-based foaming agent due to limited foaming power, experimental tests conducted in this study confirmed the feasibility of using the mixing-foaming method with the selected foaming agent and mixing system. The choice to embrace this alternative method was driven by the intention to simplify the production process and explore an innovative approach to producing 3DPFC with protein-based foaming agents.

3. Materials and methods

In the present study, two materials were prepared: a 3D-printable foamed concrete prepared using the mixing-foaming method and characterized by dry density equal to 800 ± 50 kg/m^3, referred to as 3DPFC_800; and an ultra-lightweight foamed concrete prepared using the pre-formed foaming method and characterized by dry density equal to 300 ± 50 kg/m^3, referred to as ULFC_300.

Fresh-state 2D-printability (Van Der et al., 2021) and the main hardened-state properties (drying shrinkage, compressive strength, and thermal conductivity) of 3DPFC_800 were investigated. Furthermore, the compressive strength and thermal conductivity of ULFC_300 were also investigated.

The data derived from the assessment of material properties was utilized in designing two examples of multifunctional building components based on the target thermal conductivity performance required by the UNI EN ISO 13786, as will be further elucidated later in this research paper (see **4.2**).

Finally, an application of 3DCP using 3DPFC_800 was realized by means of a robotic arm.

3.1. Materials and mix proportions

The two proposed mixes were prepared with the following ingredients: Portland cement CEM I 52.5 R in accordance with the EN 197-1 standard in terms of mix proportions of the constituting elements, a Viscosity Enhancing Agent (VEA) already employed by the authors in other works (Falliano et al., 2020b), a protein-based foaming agent, tap water, and a superplasticizer produced by *Master Builders Solutions Italia Spa*.

The mix proportions of the two different mixes presented in this study are reported in Table 1, where *w* represents water, *c* cement, *sp* superplasticizer, *fa* foaming agent (in case of mixing-foaming method), *f* foam (in case of pre-formed foaming method). When the pre-formed foaming method was employed, the pre-formed foam was produced with a concentration of the foaming agent equal to 5% in volume (Falliano et al., 2021) and was characterized by a density equal to 80 ± 5 g/l. The VEA was added in proportion to 7% and 10% of the cement weight for ULFC_300 and 3DPFC_800, respectively.

3.2. Mixture preparation

The mixing process was carried out according to two different procedures depending on the target mix. In fact, ULFC_300 was prepared according to the pre-formed foaming method, while 3DPFC_800 was prepared according to the direct mixing-foaming method.

For ULFC_300, initially, the powders were dry mixed for at least 1 min to achieve a homogeneous distribution. Subsequently, water and

Table 1
FCs employed in the present study.

Mix name	Mix proportions			
	w/c	sp/c	fa/c	f/c
3DPFC_800	45%	0.25%	3.1%	–
ULFC_300	33%	0.5%	–	56%

superplasticizer were added, and the mixture was stirred to create a cement paste. Finally, a precise amount of pre-formed foam was added, and the mixing continued until complete integration into the mixture.

For 3DPFC_800, the powders were also dry mixed initially for at least 1 min to achieve a homogeneous distribution. Subsequently, all liquids, including the foaming agent, were added, and the mixture was stirred for the necessary time to reach the target density.

In both methods, the mixing was carried out using a vertical mixer with a high mixing intensity (3000 rpm) because, as demonstrated in prior studies (Falliano et al., 2020a), (Sang et al., 2015), (Hanselmann and Windhab, 1998), the latter promotes the development of a better microstructure in the hardened-state material, due to smaller and more homogenously distributed pores, thus allowing to obtain higher mechanical performance.

The fresh state aspect of the two mixes presented in this study is shown in Fig. 1.

3.3. Research methodology

The tests conducted to characterize the materials vary between the two mixes under investigation, reflecting their distinctive properties and their designated functions within the proposed applications.

In particular, the evaluation of fresh-state 2D-printability results crucial for 3DPFC_800 to preliminarily confirm its capability to support layer-by-layer printing in the fresh state and its suitability for the envisioned robotic application. Drying shrinkage of 3DPFC_800 is also crucial for evaluating the feasibility of the proposed application and for gaining insights into the quality, especially in terms of durability and aesthetic conformity, of the final 3D-printed products. Furthermore, additional critical properties in the hardened state, such as compressive strength and thermal conductivity, need to be investigated because, in the proposed application, 3DPFC_800 serves primarily as the self-supporting material while also making a secondary contribution to thermal insulation.

In consideration of this, the subsequent properties were assessed for 3DPFC_800.

- 2D-printability. The 2D-printing test (Van Der et al., 2021) was conducted as a preliminary fresh-state printing evaluation on a smaller scale than the robotic scale used in the last part of this study. This test aimed to assess the feasibility of layering a certain number of layers, extruded through a circular nozzle with a 15 mm diameter, without any element collapse. The test involved manually operating a small tabletop extruder at a speed of approximately 15 mm/s. Throughout the experiment, different possible layer heights were explored.
- Drying shrinkage. This property was assessed using 3 prismatic specimens, measuring 4 cm × 4 cm x 16 cm, in accordance with UNI EN 12617-4 standard. After sample preparation, the specimens were kept for 24 h in molds covered with plastic foil. After 24 h, the specimens were demolded and placed in a chamber for air curing at a temperature of 21 ± 2 °C and a relative humidity of 60 ± 10%. The length measurement of the samples was conducted using a digital length comparator at intervals of 1, 4, 5, 6, 7, 14, 21, and 39 days from sample preparation.
- Compressive strength. This property was assessed using cubic specimens of 4 cm side. Two sets, each comprising 3 cubes, were utilized to evaluate compressive strength at 7 and 28 days, respectively. After 24 h from sample preparation the cubes were demolded, and prior to testing date, the specimens underwent air curing at a temperature of 20 ± 3 °C and a relative humidity of 60 ± 5%. The compressive tests were conducted in force control mode, following the UNI EN 196-1 standard, using a Zwick-Line Z050 testing machine (load capacity equal to 50 kN). The load rate, applied to the specimens perpendicularly to the casting direction, was set at 1000 N/s.
- Thermal conductivity. This property was assessed on three slabs measuring 500 mm x 500 mm x 30 mm and air cured at a temperature of 20 ± 3 °C and a relative humidity of 60 ± 5%. Before being subjected to the evaluation of the thermal conductivity, the slabs were dried in an oven until they reached a constant weight. During the test, the heat flow meter method with the cold plate set at 15 °C and the hot plate at 40 °C was employed, in alignment with previous studies by the authors (Falliano et al., 2019a) and in accordance with UNI EN 12667.
- 3D-printability. This test was conducted with the objective of prototyping the sections of the component specifically designed for this purpose, namely, the 3D-printed portions that constitute the structure of the two building components being designed, as will be explained later (see **4.2**). For the execution of this test, a Universal collaborative robotic arm, also known as a cobot, was employed. Unlike traditional industrial robots, cobots are specifically designed to collaborate safely with humans in a shared work environment, without the need for physical safety barriers. A circular-section nozzle with a diameter of 1.2 cm was employed in the printing process. To adapt continuously to some irregular flow phenomena experienced during the printing phase, the speed, initially set at an ideal 20 mm/s, was manually adjusted during the printing within the range of 10–30 mm/s.

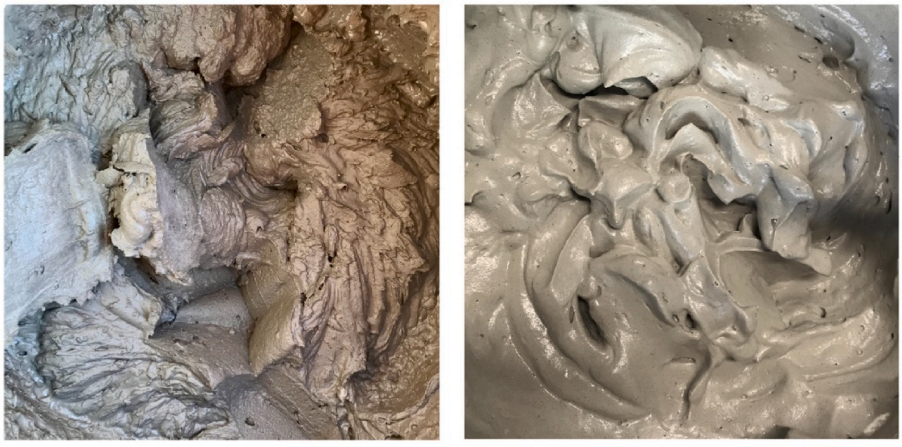

a) b)

Fig. 1. Mixtures presented in this study: a) 3DPFC_800; b) ULFC_300.

Regarding ULFC_300, as it is designed in this study to be poured into the voids defined by the previously 3D-printed material, namely 3DPFC_800, this infill material does not need to fulfill any fresh-state printability requirements, as, in the present study, it is not intended for application in 3DCP processes. Nevertheless, similar to 3DPFC_800, ULFC_300 also demands unique rheological properties tailored for its specific application, and these properties of both materials will be addressed in a forthcoming study.

In consideration of this, for ULFC_300 only the compressive strength at 7 and 28 days and thermal conductivity were assessed, and they were evaluated according to the same testing procedures described above for 3DPFC_800, with exception that, due to significantly lower expected compressive strength, the load rate applied to the specimens, perpendicularly to the direction of casting, was equal to 100 N/s.

4. Results and discussion

4.1. Preliminary material study

This section reports results related to the characterization of 3DPFC_800 and ULFC_300. As already mentioned, the tests conducted to characterize the materials vary between the two mixes under investigation, reflecting their distinctive properties and their designated functions within the proposed applications.

4.1.1. 2D-printability

The 2D-printability assessment aimed to preliminarily evaluate the potential suitability of 3DPFC_800 for 3DCP extrusion processes, as also conducted by Van Der Putten et al. (Van Der et al., 2021) and by Gao et al. (2023). As reported in Fig. 2, this test was conducted using a manually operated small-scale 2D-printing tabletop extruder, with a hand-adjusted speed of approximately 15 mm/s.

During the 2D-printing test, a continuous extrusion of 10 overlapping layers, each approximately 2.5 cm wide, was achieved without any collapse, misalignment, or buckling of the lower layers under the pressure exerted by the overlying layers. The obtained result is depicted in Fig. 3. The variations in layer height observed are not a result of deformation in the lower layers due to pressure exerted by the weight of the upper layers. Instead, they are attributed to the manual nature of the process, as illustrated in Fig. 2, and the use of this test to also try out different possible layer heights. As demonstrated in the upcoming robotic application (see **4.2**), there will be no deformation issues in the lower layers with the employed material.

Fig. 3. Result of 2D-printing test conducted on 3DPFC_800.

This method is significant, as the objective of the 2D-printing test is to evaluate the capability of 3DPFC_800 to allow the fabrication without the use of formworks sustaining a certain number of superimposed layers without any collapse, thanks to the timely development of the so-called green strength. The vertical cuts visible on the layers in Fig. 3 represent the thread pitch of the extruder used for the test. Given that the test was conducted solely to assess the 2D-printability of 3DPFC_800 and not to evaluate print quality, which will be assessed later with the 3D-printing test (see **4.2**), this extrusion system is deemed suitable for the intended purpose. The successful continuous extrusion with the overlap of 10 layers categorizes the material as printable, showcasing the excellent potential of this lightweight cementitious material, specifically 3DPFC_800, for use in 3DCP processes.

4.1.2. Hardened state properties

In addition to the 2D-printing assessment of 3DPFC_800, evaluations of some properties in the hardened state, particularly drying shrinkage on 3DPFC_800, and compressive strength and thermal conductivity on both 3DPFC_800 and ULFC_300, were conducted. For both materials, samples were prepared using the conventional methods for evaluating the properties of cementitious mortars.

The forthcoming sub-sections are dedicated to each of the hardened-state properties evaluated, namely drying shrinkage, compressive strength, and thermal conductivity.

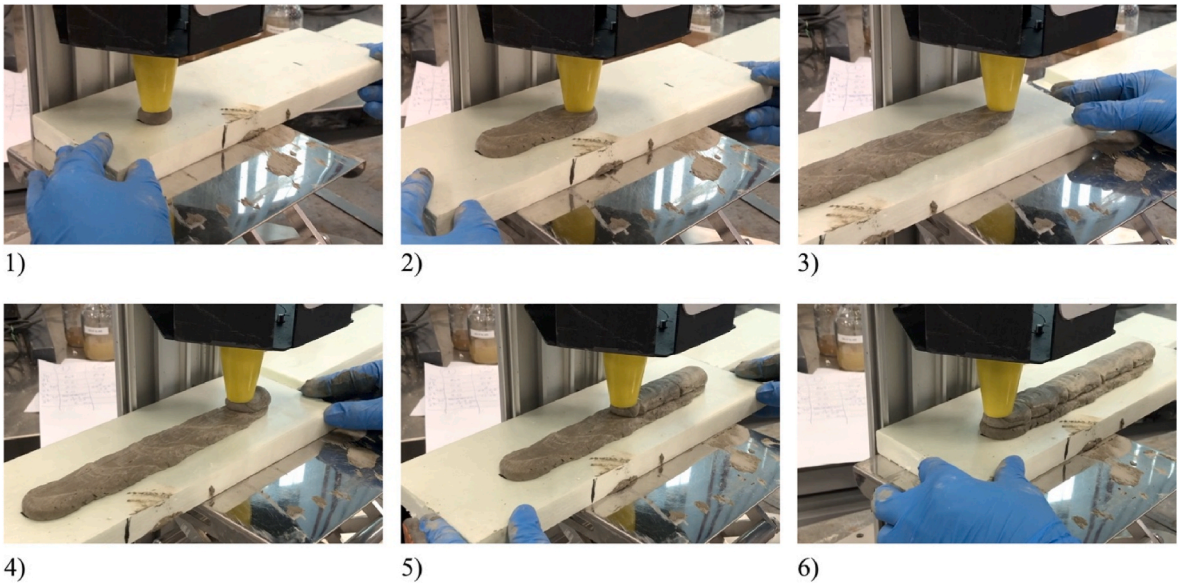

Fig. 2. Extrusion sequence of two overlapping layers using a manually operated 2D-printing tabletop extruder.

4.1.2.1. Drying shrinkage. Drying shrinkage was assessed for 3DPFC_800 on 3 prismatic specimens measuring 4 cm x 4 cm x 16 cm. The results of the test are illustrated in Fig. 4.

The evaluation of drying shrinkage is crucial as it confirms the suitability of using 3DPFC_800 for the intended application. Given that the 3D-printing process is characterized by the absence of formwork, the assessment of drying shrinkage becomes even more relevant, as this phenomenon can have adverse effects on the quality of 3D-printed products, particularly because the presence of shrinkage cracks can negatively impact their aesthetic quality and durability.

The drying shrinkage evaluation conducted on 3DPFC_800 revealed a primary shrinkage phase within the first 3 days after sample demolding, attributed to the evaporation of water contained in the samples and retained by the formwork and plastic foil before demolding and subsequent exposure to air. A notable increase in shrinkage is also observed between days 4 and 7. Lastly, a more moderate increment is consistently recorded in all subsequent measurements conducted throughout the experiment.

While the drying shrinkage characteristic of 3DPFC_800 is considered acceptable in the experimental application context of this study, further studies will be necessary to enhance the 3D-printed products in this aspect, aiming for a potential real application of the proposed building components. The formation of drying shrinkage cracks resulting from exposure to air, which, as mentioned, typically characterizes elements produced via 3D-printing, could potentially be reduced or eliminated through possible variations in the mix design, such as introducing microfibers into the mixture or specific additives tailored to such functions. The proposed solutions will undergo testing in subsequent experimental studies.

4.1.2.2. Compressive strength. Compressive strength was assessed at 7 and 28 days on cubes of 4 cm side. Specifically, for both 3DPFC_800 and ULFC_300, six cubes were prepared. Test results, along with the standard deviation and coefficient of variation, providing insight into the dispersion of the experimental findings, are presented in Table 2. The dry density of the two materials was determined by drying specimens at the age of 28 days in an oven at 110 ± 5 °C and weighing them at 24-h intervals until reaching approximately constant weight (≤1% weight loss in a 24-h period).

The 28-day compressive strength of the 3DPFC_800 series is 7.04 MPa, reflecting a 22% increase compared to the results at 7 days. Despite the different production methodology proposed and employed in this work, specifically mixing-foaming method, this value aligns well with those of foamed concretes with approximately the same density previously presented by some authors of the present paper and related to FC prepared with the pre-formed foaming method (Falliano et al., 2019a), (Falliano et al., 2020a). This trend affirms the efficacy of the mixing-foaming method for preparing low-density 3D-printable foamed concrete. Given that the compressive strength value exceeds 5 MPa, 3DPFC_800 is considered suitable for the intended function within the scope of the building components proposed in the present work. Furthermore, it is worth noting that the obtained compressive strength would enable the material to be utilized not only in the non-structural field for constructing energy-efficient building envelopes, as proposed in this work, but also in the structural domain for load-bearing structures. The latter aspect will be explored in subsequent works.

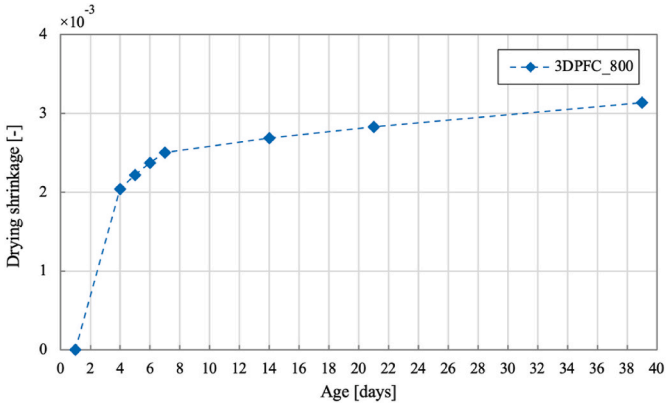

Fig. 4. Results of drying shrinkage test conducted on 3DPFC_800.

ULFC_300 also exhibits a noteworthy compressive strength value, especially considering its very low density, equal to 1.43 MPa. In this case, the increase in 28-day compressive strength compared to that at 7 days is 25%. Considering the intended role of ULFC_300 as a thermal insulator, the results found in this study open the way to the possibility of replacing this conglomerate with one characterized by an even lower density, such as the one studied by Falliano et al. (2022), which is currently undergoing evaluation for thermal performance. In fact, as seen in previous studies (Falliano et al., 2019a), the further reduction in density, thanks to increased porosity, could potentially result in better thermal performance, representing the crucial aspect for the proposed application. This possibility will be assessed in a subsequent study specifically aimed at enhancing the performance of multifunctional building components like those proposed in the present work.

4.1.2.3. Thermal conductivity. Thermal conductivity was evaluated using the heat flow meter method on three slabs of dimensions equal to 500 mm x 500 mm x 30 mm. Specifically, for both 3DPFC_800 and ULFC_300, three slabs were prepared and tested. Test results, along with the standard deviation and coefficient of variation, providing an indication of the dispersion of the experimental findings, are reported in Table 3. The dry density of the two materials was determined by drying specimens at the age of 28 days in an oven at 110 ± 5 °C and weighing them at 24-h intervals until reaching approximately constant weight (≤1% weight loss in a 24-h period).

The results indicate that reducing the target density from 800 kg/m^3 to 300 kg/m^3 leads to a percentage decrease in the thermal conductivity of approximately 65%. Indeed, the reduction in density results in an increase of porosity and, consequently, enhanced thermal insulation properties (Falliano et al., 2019a).

The obtained results align with the application objectives of the two materials envisioned in the present study for the development of multifunctional building components as detailed in the following section (see **4.2**): in fact, ULFC_300 is specifically designed to primarily fulfill the thermal performance of the component. However, since 3DPFC_800 also possesses a certain level of porosity, even if significantly lower than ULFC_300, it also contributes to the overall assessment of the thermal performance of the proposed building components.

Also regarding the thermal conductivity, despite the different production methodology proposed and employed in this study for 3DPFC_800, namely the mixing-foaming method, the obtained values align well with those of foamed concretes with approximately the same density presented previously by some authors of this paper, and related to FC prepared with the pre-formed foaming method (Falliano et al., 2019a). These results further confirm the efficacy of the mixing-foaming method for preparing low-density 3D-printable foamed concrete.

Based on the obtained results, it can be stated that, in addition to density reduction of the infill material as proposed in the preceding subsection, a potential future direction for the research could involve defining a 3D-printable foamed conglomerate with a lower density, presumably around 600 kg/m^3, capable of achieving a thermal conductivity lower than 0.14 W/mK, thus offering a higher contribution in thermal performance. However, it is also essential to take into account the compressive strength requirements discussed earlier in the previous sub-section, which are considered essential for the proposed application of 3DPFC_800.

The thermal properties presented in the experimental results have

Table 2
Experimental 7-day and 28-day compressive strength referred to 3DPFC_800 and ULFC_300.

mix name	Compressive strength						
	mean dry density γdry [kg/m^3]	mean 7-day compr. strength $R_{c,7d,m}$ [MPa]	standard deviation [MPa]	coefficient of variation [−]	mean 28-day compr. strength $R_{c,28d,m}$ [MPa]	standard deviation [MPa]	coefficient of variation [−]
3DPFC_800	820	5.75	0.17	0.03	7.04	0.11	0.02
ULFC_300	305	1.14	0.06	0.05	1.43	0.05	0.03

Table 3
Experimental thermal conductivity referred to 3DPFC_800 and ULFC_300.

mix name	Thermal conductivity			
	mean dry density γdry [kg/m^3]	mean thermal conductivity λ [W/mK]	standard deviation [W/mK]	coefficient of variation [−]
3DPFC_800	793	0.205	0.00075	0.0036
ULFC_300	315	0.072	0.00081	0.0112

been utilized to design the innovative building elements, as detailed in the following section (see **4.2**).

4.2. Design of multifunctional building components and 3DCP application

The proposed design methodology, which aims to create multifunctional building components with customizable properties by exploiting the synergy among different densities of FCs and implementing 3DCP, is applied in a case study. Specifically, in this study, the methodology is employed for designing building components for energy efficiency interventions on the opaque envelope of existing buildings, with the goal of improving thermal performance while simultaneously ensuring an aesthetically renovated façade. The study focuses on buildings situated in climate zone E within the Italian context, which applies to the majority of Italian municipalities. According to the local regulatory framework outlined in DPR 412/1993, the climatic zone E exhibits a range of heating degree days spanning from 2101 to 3000. The characteristics of the assumed existing walls, which are 30-cm-thick uninsulated hollow brick walls, are detailed in Table 4.

Applying the proposed design methodology has resulted in the definition of two types of building components utilizing 3DPFC_800 and ULFC_300: a tongue-and-groove block suitable for production in prefabrication plants and subsequent on-site assembly (hereafter referred to as BC.1); and a solution designed for direct printing at the construction site (hereafter referred to as BC.2). In both scenarios, the components consist of 3D-printed elements, 3DPFC_800, serving as the structural part and disposable formwork, complemented by ULFC_300 to fill the cavities defined by the former.

It is essential to highlight that the explored application represents just one of the potential uses of the proposed design approach, and the components presented in this section serve as examples of what can be achieved by applying this method, using the experimental results previously reported in this study as a basis. The design process described here for two building components made of the two materials investigated (see **4.1**) could lead to several more formally and/or functionally complex solutions designed for other types of applications.

Lastly, an application of 3DCP employing 3DPFC_800 is presented, and potential solutions to address certain process issues and prevent defects on the final components are suggested.

Table 4
Thermal parameters related to the existing uninsulated hollow brick face wall.

Thermal performance according to UNI EN ISO 13786				
stationary thermal transmittance U [W/m^{2}K]	surface density [kg/m^3]	periodic thermal transmittance Y_{ie} [W/m^{2}K]	decrement factor [−]	time shift [h]
0.918	248	0.366	0.399	8.57

4.2.1. Design

Once the key properties of 3DPFC_800 and ULFC_300 were established, the formal and functional optimization of the building components focused primarily on the thermal performance of the building envelope, including both the existing wall and the newly designed components. Specifically, the objective was to achieve two main goals: eliminating any thermal bridges and ensuring compliance with the maximum limits established by the Italian regulation DM June 26, 2015 for the stationary thermal transmittance of the building envelope in the specific application under consideration, set at 0.28 W/m^{2}K.

Although the section design of the components was based on these two goals, many other aspects were taken into consideration during this phase as well. For instance, in the design phase, special attention has been given to optimizing the path of the 3D-printed layer, which was assumed to have a width of 25 mm based on the specifications of the nozzle associated with the robotic system used for 3D-printing, as will be explained later (see **4.2**). This includes considerations such as ensuring the continuity of the printing path, managing the angles of directional changes, and reinforcing the component by incorporating an internal printing path to prevent the presence of excessively long free path segments to avoid possible instability issues. Additionally, durability aspects have been addressed by guaranteeing the continuity of the extruded layer on exposed faces. Simultaneously, efforts were made to define closed perimeters for the pouring of the infill ULFC_300. Furthermore, in addition to the stationary thermal transmittance, other thermal parameters have been assessed using the UNI EN ISO 13786 standard (specifically periodic thermal transmittance, decrement factor, time shift, and surface density) and have been taken into consideration. Lastly, only for the component designed for prefabrication in the factory and subsequent assembly on site, some limitations have been imposed (based on building components for similar uses currently on the market) on their size and weight to ensure ease of transport and handling, and to facilitate assembly operations in the scenario of a real application of these components. In particular, a maximum size of 50 cm in the three directions and a maximum weight of 10 kg were imposed.

Building components, BC.1 and BC.2, designed according to the principles mentioned above, are illustrated in Figs. 5 and 6, and Figs. 7 and 8, respectively. Their thermal characteristics are detailed in Table 5 and Table 6, respectively.

Upon comparing the thermal data presented in Table 4, Tables 5 and 6, both solutions were proven effective in achieving excellent thermal performance, with BC.1 exhibiting superior characteristics in this regard. In fact, through the implementation of the proposed solutions the thermal transmittance U of the building envelope can be significantly enhanced, bringing it back within the permissible range defined by the relevant standard, specifically 28 W/m^{2}K. In particular, an average percentage increase of 244% and 245% can be obtained in the case of BC.1 and BC.2, respectively, compared to the existing wall. Moreover, the adopted solutions lead to improvements in other thermal parameters considered. For instance, they also contribute to enhancing the thermal performance under dynamic conditions by increasing the thermal inertia of the system through a rise in surface density. Additionally, there is a substantial reduction in the impact of external thermal flow on internal environments, achieved through a decrease in the decrement

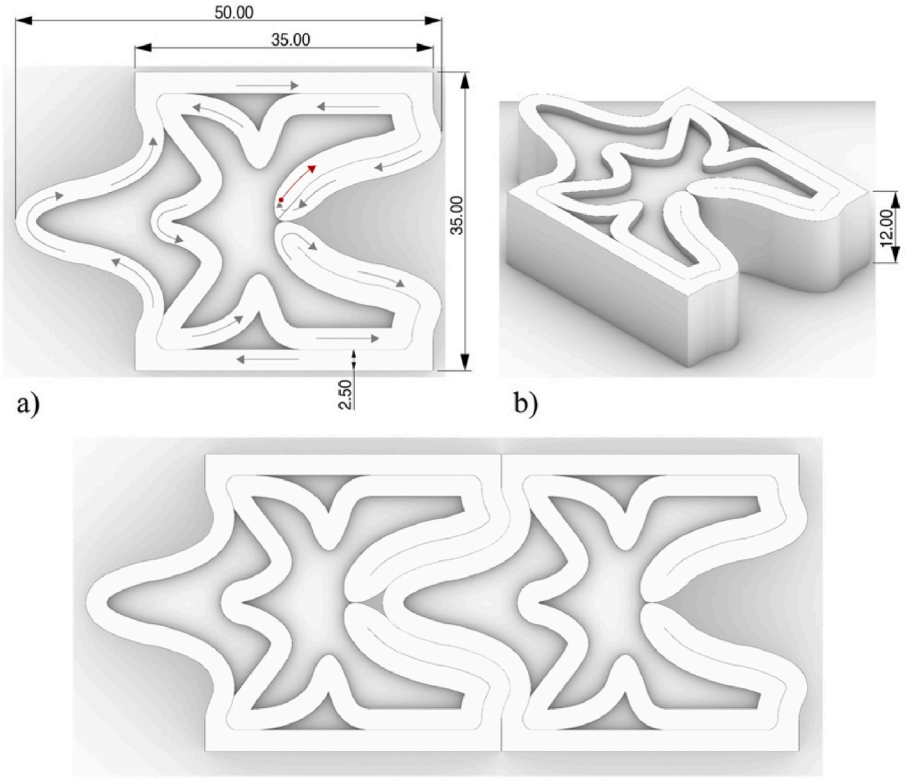

Fig. 5. BC.1 design: a) horizontal section with representation of the printing path; b) isometric 3D view; c) tongue and groove between two blocks. (All measures are in cm).

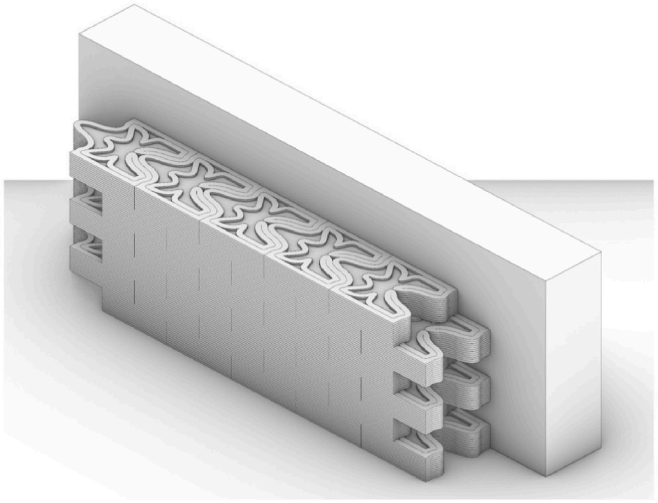

Figs. 6. 3D isometric representation of BC.1 applied to the existing wall.

factor and time shift. As previously stated regarding the properties of the investigated materials (see **4.1**), to achieve even better performance, it would be possible to employ materials with higher thermal efficiency. Specifically, consideration could be given to using more thermally advanced materials, especially for the ultra-lightweight material intended for filling the voids, which plays a key role in the thermal properties of the new components.

From a methodological standpoint, one potential improvement could involve the implementation of parametric design.

In fact, this design methodology is particularly compelling in the case of 3DCP applications due to its potential for the unitary management of the entire design and realization process, and the possible management of highly complex geometries through a relatively simple tool. It also provides the ability to modify the component in progress quickly and easily by adjusting input design parameters, facilitating rapid design adaptation, and offering a cost-effective solution tailored to the specific case, thereby making the method even more flexible. Furthermore, through the use of parametric design, it would be possible to optimize the design of building components based on specific requirements while meeting regulatory standards. An example of some potential modifications that could be implemented instantly and cost-efficiently by adopting parametric design for the design of the BC.2 component is illustrated in Fig. 9.

4.2.2. Robotic application

Once the building components were defined, an application of 3DCP was carried out using the material specifically designed for this type of application, namely 3DPFC_800. For this purpose, as illustrated in Fig. 10, a Universal collaborative robot with a nozzle of 12 mm diameter circular section (resulting in an extruded layer approximately 25 mm wide and 10 mm high) was employed.

Regarding BC.2, which, as previously mentioned, relates to a possible on-site application, only a portion with a length of 35 cm was realized during the 3DCP test. This choice is linked to the desire to limit the printed object's size to promote its handling while still demonstrating its technical feasibility. To distinguish the graphic representations, this modified solution is referred to as BC.2.1 and its design is shown in Fig. 11. Nevertheless, it should be emphasized that in the actual scenario, this modified solution should not be characterized by the straight transverse closure on both short sides of the element, since, despite its low density, it might result in a thermal bridge; instead, the continuity of the element around the entire perimeter of the building's exterior walls, in the case of real on-site application, would avoid the possible thermal bridge phenomenon here highlighted.

The outcomes of the 3DCP applications for the high-density portions

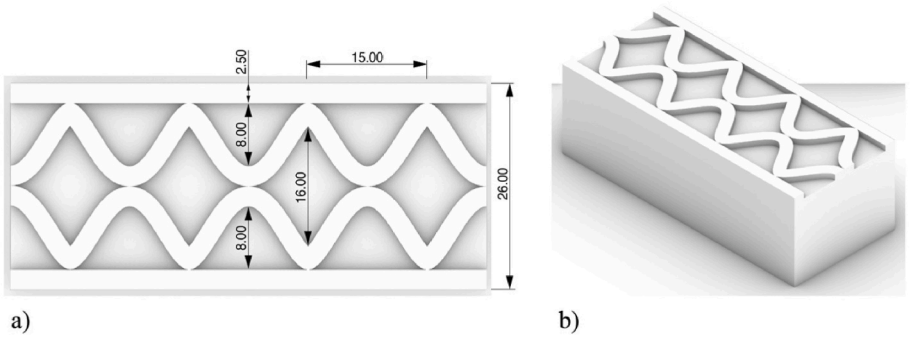

Fig. 7. BC.2 design: a) horizontal section; b) isometric 3D view. (All measures are in cm).

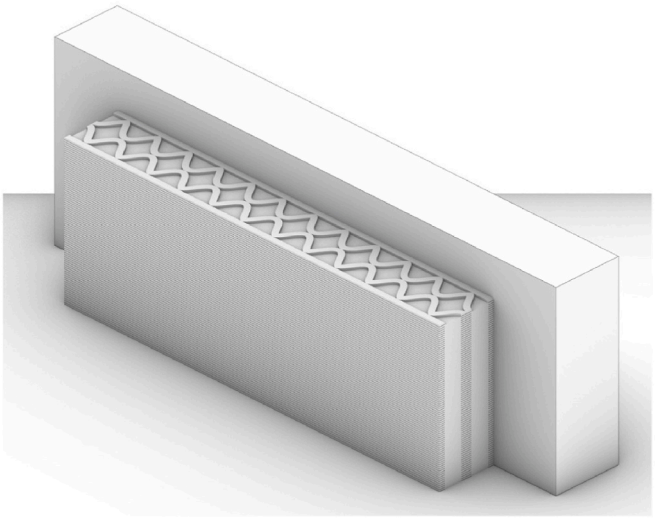

Figs. 8. 3D isometric representation of BC.2 applied to the existing wall.

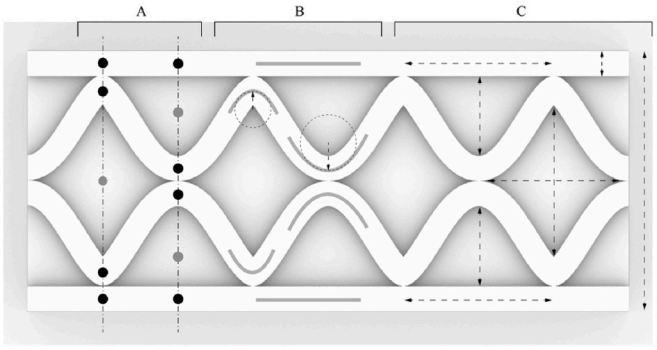

Fig. 9. Exemplification of some types of parameters that could be instantly modified using parametric design to customize and optimize building components. A: stratigraphy of the individual section, succession of a number of high-density printed layers and infill cavities; B: orientation of printed layers and radius of curvature of curvilinear sections; C: thickness of printed layers, size of cavities defined by printed path, and resulting total thickness of the element being designed.

Table 5
Thermal parameters related to the complete system, including the existing wall and BC.1. All data are average values of the sections evaluated. (*the value in each section is always lower than 0.28 W/m^{2}K).

Thermal performance according to UNI EN ISO 13786:2008				
stationary thermal transmittance U [W/m^{2}K]	surface density [kg/m^3]	periodic thermal transmittance Y_{ie} [W/m^{2}K]	decrement factor [−]	time shift [h]
0.267*	473	0.0034	0.013	>24

Table 6
Thermal parameters related to the complete system, including the existing wall and BC.2. All data are average values of the sections evaluated. (*the value in each section is always lower than 0.28 W/m^{2}K).

Thermal performance according to UNI EN ISO 13786				
stationary thermal transmittance U [W/m^{2}K]	surface density [kg/m^3]	periodic thermal transmittance Y_{ie} [W/m^{2}K]	decrement factor [−]	time shift [h]
0.266*	376	0.010	0.038	20.14

of BC.1 and BC.2.1 are illustrated in Figs. 12 and 13.

The 3D-printing trials confirmed the effective applicability of 3DPFC_800 in 3DCP processes, experimentally validating its suitable properties for efficient pumping, extrusion, and layer-by-layer 3D-printing. Significantly, following extrusion, the material demonstrates the capacity to promptly establish green strength, allowing it to support a certain number of overlying layers while maintaining its shape unaltered and ensuring the stability of the component. This is evident from the absence of deformations in the lower layers under the weight of those above. Following these tests, 3DPFC_800 was deemed suitable for 3DCP applications, without the need for formworks, for creating 3D-printed elements composed of overlapping layers, and this outcome underscores the exceptional potential of the lightweight cementitious material, particularly 3DPFC_800, for integration into 3DCP processes.

Nonetheless, the 3D-printing tests also revealed some practical challenges that require further attention in the realm of 3DCP with FC. In fact, both during the process and the subsequent qualitative analyses of the printed elements, several issues and defects have been identified.

Concerning the process, several issues were encountered during the fabrication of the components, and among these, the main ones include: irregular extruded flow with occasional interruptions during the printing process, likely caused by sporadic macro-air bubble occurrences; occasional presence of tearing in printed filaments due to poor fluidity of the material; slippages of printed material outside the printing path in cases of excessive material fluidity. These issues primarily originated from the non-uniformity of material consistency and fluidity, possibly influenced by the waiting time between material mixing and actual extrusion, as well as irregular material flow due to pumping issues and the presence of macro-air bubbles.

As a temporary measure during the production process, the initially planned constant printing speed of 20 mm/s was manually adjusted to a range between 10 mm/s and 30 mm/s to accommodate the irregular material flow from the nozzle. Another potential solution to address challenges related to pumping and reduce the presence of macro-air bubbles involves greater control of pump pressure and testing the

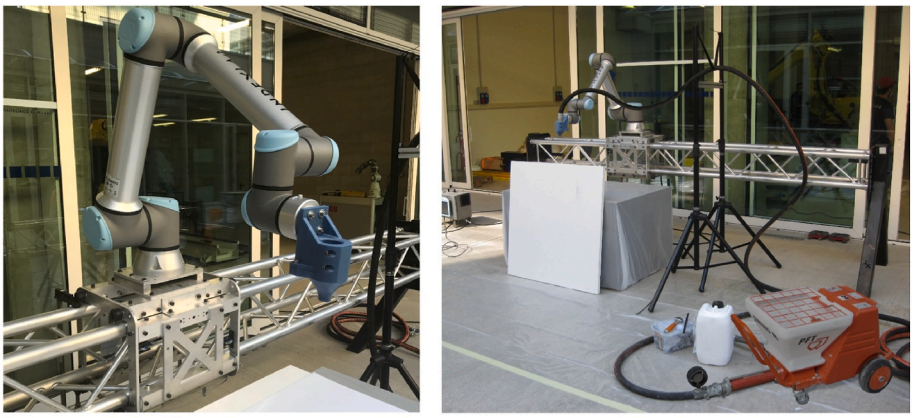

Fig. 10. Robotic system employed for prototyping: a) collaborative robot; b) entire system consisting of pump, hose, and robot.

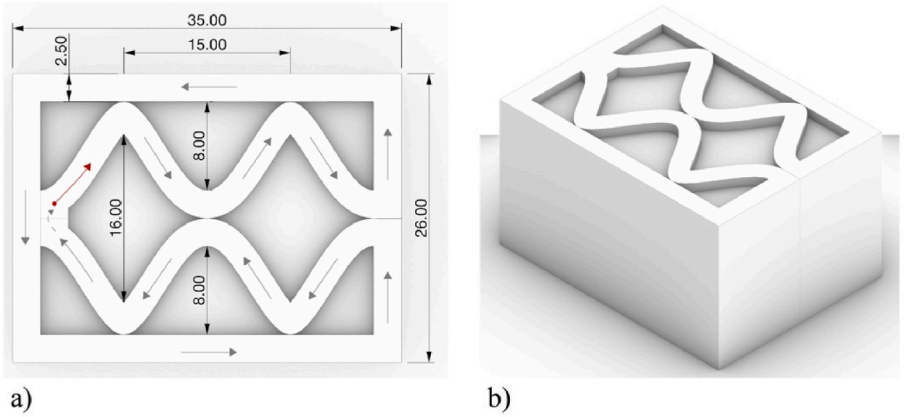

Fig. 11. BC.2.1 design: a) horizontal section with representation of the printing path; b) isometric 3D view. (All measures are in cm).

Fig. 12. Representative images of BC.1 obtained using 3DCP.

implementation of an extruder at the printing head, just before the nozzle. Certainly, the process phase plays a crucial role as it directly impacts the final element's properties, performance, and quality in the hardened state, so this phase must be carefully considered for possible improvements in results. The proposed solutions and other potential remedies for addressing the highlighted process issues will undergo testing in subsequent practical experimental studies.

Lastly, a qualitative evaluation of the components in the hardened state allowed to assess the final characteristics of BC.1 and BC.2.1, specifically focusing on geometric conformity to the design, potential defects in the layers, adhesion between overlapping layers, and the overall aesthetics. The final characteristics of the components in the hardened state, along with the results of this qualitative evaluation, are detailed in Table 7.

During the qualitative evaluation of the building components, the height of the printed elements was recorded. This assessment revealed a correspondence between the expected and final height of the elements, further confirming the buildability property of 3DPFC_800 and the absence of deformations in the lower layers, which are subjected to greater pressure due to the weight of the overlying ones.

Three types of defects due to the fabrication process and observed on the final components are highlighted in Fig. 14. These defects, representing the main issues of the manufactured elements and directly deriving from the aforementioned process issues, include slippages out of the printing path due to excessive localized fluidity, presence of tearing due to the lack of continuity in the printed filament caused by localized fluidity reductions, and the presence of cavities and cracks due to the creation of macro-bubbles during the production process. No

Fig. 13. Representative images of BC.2.1 obtained using 3DCP.

Table 7
General characteristics of the 3D-printed objects. (*this characteristic was evaluated by breaking the element).

Final characteristics of extruded components		
	BC.1	BC.2.1
layer height	12 mm	12 mm
layer width	24–30 mm	24–30 mm
total element height	120 mm	168 mm
number of fully realized levels	10	13
number of levels even only partially realized	10	14
surface features defects	homogeneous and opaque localized slippages, tearing, macro-bubbles cavities	homogeneous and opaque localized slippages, tearing, macro-bubbles cavities
*adhesion between layers (no cold joints)**	yes	yes

cracks due to drying shrinkage were visually detected in the manufactured building components. However, possible variations in the mix design, such as introducing microfibers into the mixture or incorporating specific additives tailored to such functions, could further mitigate the occurrence of the phenomenon, which typically characterizes 3D-printed elements due to the absence of formwork. All the aforementioned solutions will be subjected to testing in subsequent practical experimental studies.

5. Conclusions and outlook

This study introduces the concept of exploiting synergies from the combined utilization of foamed concretes (FCs) with varying densities and 3D Concrete Printing (3DCP) to create innovative and highly optimized multifunctional building components. The potential of this proposed design methodology is exemplified through the development of two sample components tailored for energy-efficient interventions in existing buildings.

The design of the proposed sample components involves the integrated use of 3D-printable foamed concrete with a targeted dry density of 800 kg/m^3 (3DPFC_800), primarily serving a structural function, and ultra-lightweight foamed concrete with a targeted dry density of 300 kg/m^3 (ULFC_300), primarily acting as filling for the voids defined by the former. This innovative approach ensures the achievement of both high mechanical performance and excellent thermal insulation using a single component characterized by the same cementitious matrix.

Upon defining key properties such as 2D-printability and drying shrinkage for 3DPFC_800, and compressive strength and thermal conductivity for both 3DPFC_800 and ULFC_300, the obtained data were leveraged to design two examples of multifunctional building components, aligning with the desired thermal performance targets. Finally, a practical application of 3DCP using 3DPFC_800 was executed with the assistance of a robotic arm.

Based on the experimental study, the following conclusions can be drawn.

1) 3DPFC_800 has been successfully produced using the mixing-foaming method. Although this method is not commonly used for the production of 3D-printable foamed concrete, it has proven effective with the production method and foaming agent employed in this study.
2) 3DPFC_800 is characterized by a compressive strength at 28 days of 7.04 MPa. The material is, therefore, suitable for the use envisaged in this research study, and it could also be used in the structural field;
3) considering its very low density, ULFC_300 is also characterized by a non-negligible compressive strength equal to 1.43 MPa. This finding

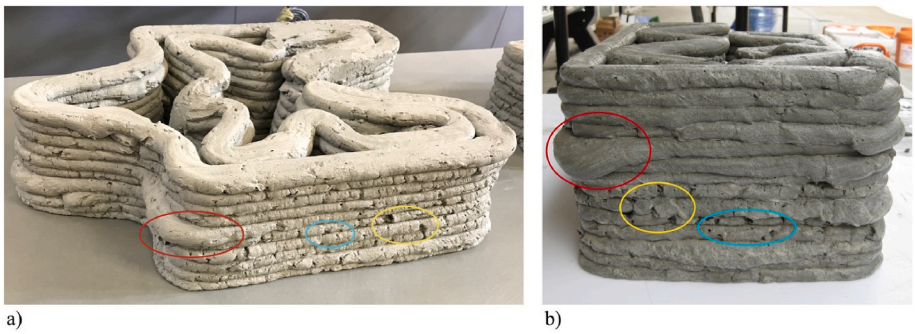

Fig. 14. Examples of defects due to the manufacturing process: a) hardened-state BC.1; b) fresh-state BC.2.1. Slippage out of the printing path, tearings on single layers, and cavities or craks left by the presence of macro air bubbles are highlighted in red, yellow and blue circles, respectively. (For interpretation of the references to colour in this figure legend, the reader is referred to the Web version of this article.)

leaves the way open to the possibility of replacing this conglomerate with one characterized by an even lower density in the context of the proposed building components;

4) 3DPFC_800 and ULFC_300 are characterized by a thermal conductivity equal to 0.205 W/mK and 0.072 W/mK, respectively, with a percentual decrease of the latter compared to the former of about 65%. Therefore, ULFC_300 can be considered an insulating material. In future studies, it would be interesting to produce a 3D-printable foamed concrete characterized by lower density to increase the thermal performance of the resistant portion of the proposed multifunctional components as well;
5) the possibility to achieve by continuous extrusion the overlap of 10 layers without collapse, misalignment and buckling phenomena makes 3DPFC_800 a printable material suitable for 3DCP applications;
6) 3DPFC_800 was successfully employed in a 3DCP printability tests. These tests revealed both the strengths and the issues, defects, and challenges that still need to be addressed in the field of 3DCP with foamed concrete. Some potential solutions to the highlighted issues have been proposed, and further studies will be necessary to thoroughly investigate these problems, ensuring the development of high-performance products.

Funding sources

The PhD work of Silvia Parmigiani is funded by the Italian Programma Operativo Nazionale (PON) “Ricerca e Innovazione” 2014–2020, Asse IV “Istruzione e ricerca per il recupero”, Azione IV.5 “Dottorati su tematiche green” DM 1061/2021.

The work of Devid Falliano was carried out within the Ministerial Decree no. 1062/2021 and received funding from the FSE REACT-EU – PON Ricerca e Innovazione 2014–2020.

CRediT authorship contribution statement

Silvia Parmigiani: Writing – review & editing, Writing – original draft, Methodology, Investigation, Formal analysis, Data curation. **Devid Falliano:** Writing – review & editing, Writing – original draft, Methodology, Investigation, Formal analysis, Data curation, Conceptualization. **Sandro Moro:** Visualization, Methodology, Investigation. **Giuseppe Andrea Ferro:** Writing – review & editing, Validation, Supervision. **Luciana Restuccia:** Writing – review & editing, Validation, Supervision, Methodology, Conceptualization.

Declaration of competing interest

The authors declare that they have no known competing financial interests or personal relationships that could have appeared to influence the work reported in this paper.

Data availability

Data will be made available on request.

Acknowledgments

The authors wish to thank the company IndexLab and, in particular, Dr. Pierpaolo Ruttico for the valuable partnership and for providing the robotic arm for making the 3DCP application; additionally, the authors wish to thank Mr. Ernesto Gugliandolo for his support and valuable suggestions during the research activities and Dr. Daniel Suarez-Riera for his help with 3D-printing procedures.

References

Asprone, D., Menna, C., Bos, F.P., Salet, T.A.M., Mata-Falcón, J., Kaufmann, W., 2018. Rethinking reinforcement for digital fabrication with concrete. Cement Concr. Res. 112, 111–121. https://doi.org/10.1016/j.cemconres.2018.05.020.

Boddepalli, U., Gandhi, I.S.R., Panda, B., 2023. Stability of three-dimensional printable foam concrete as function of surfactant characteristics. Front. Struct. Civ. Eng. 17 (6), 935–947. https://doi.org/10.1007/s11709-023-0964-z.

Bos, F., Wolfs, R., Ahmed, Z., Salet, T., 2016. Additive manufacturing of concrete in construction: potentials and challenges of 3D concrete printing. Virtual Phys. Prototyp. 11 (3), 209–225. https://doi.org/10.1080/17452759.2016.1209867.

Buswell, R.A., Leal de Silva, W.R., Jones, S.Z., Dirrenberger, J., 2018. 3D printing using concrete extrusion: a roadmap for research. Cement Concr. Res. 112, 37–49. https://doi.org/10.1016/j.cemconres.2018.05.006.

Chen, M., Liu, B., Li, L., Cao, L., Huang, Y., Wang, S., Zhao, P., Lu, L., Cheng, X., 2020. Rheological parameters, thixotropy and creep of 3D-printed calcium sulfoaluminate cement composites modified by bentonite. Compos. Part B. 186, 107821. https://doi.org/10.1016/j.compositesb.2020.107821.

Chica, L., Alzate, A., 2019. Cellular concrete review: new trends for application in construction. Construct. Build. Mater. 200, 637–647. https://doi.org/10.1016/j.conbuildmat.2018.12.136.

Cho, S., Kruger, J., Zeranka, S., Van Rooyen, A., Van Zijl, G., 2019. Mechanical evaluation of 3D printable nano-silica incorporated fiber-reinforced lightweight foam concrete. In: Proceedings of the 10th International Conference on Fracture Mechanics of Concrete and Concrete Structures (FRAMCOS-X). https://doi.org/10.21012/FC10.232696.

Cho, S., Kruger, J., Von Rooyen, A., Zeranka, S., Van Zijl, G., 2020. Rheology of 3D printable lightweight foam concrete incorporating nano-silica. In: Rheology and Processing of Construction Materials – RheoCon2 & SCC9, RILEM Bookseries 23. Springer, Cham, pp. 373–381. https://doi.org/10.1007/978-3-030-22566-7_43.

Cho, S., Kruger, J., van Rooyen, A., van Zijl, G., 2021. Rheology and application of buoyant foam concrete for digital fabrication. Compos. Part B. 215, 108800. https://doi.org/10.1016/j.compositesb.2021.108800.

Cho, S., Van Rooyen, A., Kearsley, E., Van Zijl, G., 2022. Foam stability of 3D printable foamed concrete. J. Build. Eng. 47, 103884. https://doi.org/10.1016/j.jobe.2021.103884.

De Schutter, G., Lesage, K., Mechtcherine, V., Naidu Nerella, V., Habert, G., Agusti-Juan, I., 2018. Vision of 3D Printing with concrete – technical, economic and environmental potentials. Cement Concr. Res. 112, 25–36. https://doi.org/10.1016/j.cemconres.2018.06.001.

du Plessis, A., Babafemi, A.J., Paul, S.C., Panda, B., Tran, J.P., Broeckhoven, C., 2021. Biomimicry for 3D concrete printing: a review and perspective. Addit. Manuf. 38, 101823. https://doi.org/10.1016/j.addma.2020.101823.

Falliano, D., De Domenico, D., Ricciardi, G., Gugliandolo, E., 2018. Experimental investigation on the compressive strength of foamed concrete: effect of curing conditions, cement type, foaming agent and dry density. Construct. Build. Mater. 165, 735–749. https://doi.org/10.1016/j.conbuildmat.2017.12.241.

Falliano, D., Gugliandolo, E., De Domenico, D., Ricciardi, G., 2019a. Experimental investigation on the mechanical strength and thermal conductivity of extrudable foamed concrete and preliminary views on its potential application in 3D printed multilayer insulating panels. In: Wangler, T., Flatt, R.J. (Eds.), First RILEM International Conference on Concrete and Digital Fabrication – Digital Concrete 2018, RILEM Bookseries, 19. Springer, Cham, pp. 277–286. https://doi.org/10.1007/978-3-319-99519-9_26.

Falliano, D., Sciarrone, A., De Domenico, D., Maugeri, N., Longo, P., Gugliandolo, E., Ricciardi, G., 2019b. Fiber-reinforced lightweight foamed concrete panels suitable for 3D printing applications. In: IOP Conf. Ser.: Mater. Sci. Eng., 615, 012018. https://doi.org/10.1088/1757-899X/615/1/012018.

Falliano, D., De Domenico, D., Ricciardi, G., Gugliandolo, E., 2020a. 3D-printable lightweight foamed concrete and comparison with classical foamed concrete in terms of fresh state properties and mechanical strength. Construct. Build. Mater. 254, 119271. https://doi.org/10.1016/j.conbuildmat.2020.119271.

Falliano, D., Crupi, G., De Domenico, D., Ricciardi, G., Restuccia, L., Ferro, G., Gugliandolo, E., 2020b. Investigation on the rheological behavior of lightweight foamed concrete for 3D printing applications. In: Second RILEM International Conference on Concrete and Digital Fabrication – Digital Concrete 2020, RILEM Bookseries, 28. Springer, Cham, pp. 246–254. https://doi.org/10.1007/978-3-030-49916-7_25.

Falliano, D., Restuccia, L., Gugliandolo, E., 2021. A simple optimized foam generator and a study on peculiar aspects concerning foams and foamed concrete. Construct. Build. Mater. 268, 121101. https://doi.org/10.1016/j.conbuildmat.2020.121101.

Falliano, D., Parmigiani, S., Suarez-Riera, D., Ferro, G.A., Restuccia, L., 2022. Stability, flexural behavior and compressive strength of ultra-lightweight fiber-reinforced foamed concrete with dry density lower than 100 kg/m^3. J. Build. Eng. 51, 104329. https://doi.org/10.1016/j.jobe.2022.104329.

Fu, Y., Wang, X., Wang, L., Li, Y., 2020. Foam concrete: a state-of-the-art and state-of-the-practice review. Adv. Mater. Sci. Eng. 2020, 6153602. https://doi.org/10.1155/2020/6153602.

Gao, Y., Hua, S., Yue, H., 2023. Study on preparation and rheological properties of 3D printed pre-foaming concrete. Appl. Sci. 13, 5303. https://doi.org/10.3390/app13095303.

Geng, Z., Pan, H., Zuo, W., She, W., 2022. Functionally graded lightweight cement-based composites with outstanding mechanical performances via additive manufacturing. Addit. Manuf. 56, 102911. https://doi.org/10.1016/j.addma.2022.102911.

Gopalakrishnan, R., Sounthararajan, V.M., Mohan, A., Tholkapiyan, M., 2020. The strength and durability of fly ash and quarry dust light weight foam concrete. Mater. Today Proc. 22, 1117–1124. https://doi.org/10.1016/j.matpr.2019.11.317.

Gosselin, C., Duballet, R., Roux, Ph, Gaudilliére, N., Dirrenberger, J., Morel, Ph, 2016. Large-scale 3D printing of ultra-high performance concrete – a new processing route for architects and builders. Mater. Des. 100, 102–109. https://doi.org/10.1016/j.matdes.2016.03.097.

Hanselmann, W., Windhab, E., 1998. Flow characteristics and modelling of foam generation in a continuous rotor/stator mixer. J. Food Eng. 38 (4), 393–405. https://doi.org/10.1016/S0260-8774(98)00129-0.

Hashim, M., Tantray, M., 2021. Comparative study on the performance of protein and synthetic-based foaming agents used in foamed concrete. Case Stud. Constr. Mater. 14, e00524. https://doi.org/10.1016/j.cscm.2021.e00524.

Jiang, J., Lu, Z., Niu, Y., Li, J., Zhang, Y., 2016. Study on the preparation and properties of high-porosity foamed concretes based on ordinary Portland cement. Mater. Des. 92, 949–959. https://doi.org/10.1016/j.matdes.2015.12.068.

Jones, M.R., Ozlutas, K., Zheng, L., 2016. Stability and instability of foamed concrete. Mag. Concr. Res. 1500097. https://doi.org/10.1680/macr.15.00097.

Jones, M.R., Ozlutas, K., Zheng, L., 2017. High-volume, ultra-low-density fly ash foamed concrete. Mag. Concr. Res. 69 (22), 1700063. https://doi.org/10.1680/jmacr.17.00063.

Kearsley, E.P., Wainwright, P.J., 2002. The effect of porosity on the strength of foamed concrete. Cement Concr. Res. 32, 233–239. https://doi.org/10.1016/S0008-8846(01)00665-2.

Khan, M.S., Sanchez, F., Zhou, H., 2020. 3-D printing of concrete: beyond horizons. Cement Concr. Res. 133, 106070. https://doi.org/10.1016/j.cemconres.2020.106070.

Lim, S., Buswell, R.A., Le, T.T., Austin, S.A., Gibb, A.G.F., Thorpe, T., 2012. Developments in construction-scale additive manufacturing processes. Autom. ConStruct. 21, 262–268. https://doi.org/10.1016/j.autcon.2011.06.010.

Liu, C., Wang, X., Chen, Y., Zhang, C., Ma, L., Deng, Z., Chen, C., Zhang, Y., Pan, J., Banthia, N., 2021. Influence of hydroxypropyl methylcellulose and silica fume on stability, rheological properties, and printability of 3D printing foam concrete. Cement Concr. Compos. 122, 104158. https://doi.org/10.1016/j.cemconcomp.2021.104158.

Liu, C., Chen, Y., Xiong, Y., Jia, L., Ma, L., Wang, X., Chen, C., Banthia, N., Zhang, Y., 2022a. Influence of HPMC and SF on buildability of 3D printing foam concrete: from water state and flocculation point of view. Compos. Part B. 242, 110075. https://doi.org/10.1016/j.compositesb.2022.110075.

Liu, C., Xiong, Y., Chen, Y., Jia, L., Ma, L., Deng, Z., Wang, Z., Chen, C., Banthia, N., Zhang, Y., 2022b. Effect of sulphoaluminate cement on fresh and hardened properties of 3D printing foamed concrete. Compos. Part B. 232, 109619. https://doi.org/10.1016/j.compositesb.2022.109619.

Liu, C., Zhang, Y., Banthia, N., 2023. Unveiling pore formation and its influence on mechanical property and stress distribution of 3D printed foam concrete modified with hydroxypropyl methylcellulose and silica fume. Addit. Manuf. 71, 103606. https://doi.org/10.1016/j.addma.2023.103606.

Lublasser, E., Adams, T., Vollpracht, A., Brell-Cokcan, S., 2018. Robotic application of foam concrete onto bare wall elements – analysis, concept and robotic experiments. Autom. ConStruct. 89, 299–306. https://doi.org/10.1016/j.autcon.2018.02.005.

Marais, H., Christen, H., Cho, S., De Villiers, W., Van Zijl, G., 2021. Computational assessment of thermal performance of 3D printed concrete wall structures with cavities. J. Build. Eng. 41, 102431. https://doi.org/10.1016/j.jobe.2021.102431.

Markin, V., Nerella, V.N., Schröfl, C., Guseynova, G., Mechtcherine, V., 2019a. Material design and performance evaluation of foam concrete for digital fabrication. Materials 12 (15), 2433. https://doi.org/10.3390/ma12152433.

Markin, V., Sahmenko, G., Nerella, V.N., Näther, M., Mechtcherine, V., 2019b. Investigations on the foam concrete production techniques suitable for 3D-printing with foam concrete. In: IOP Conf. Series: Mater Sci. Eng., 660, 012039. https://doi.org/10.1088/1757-899X/660/1/012039.

Markin, V., Ivanova, I., Fataei, S., Reißig, S., Mechtcherine, V., 2020. Investigation on structural build-up of 3D printable foam concrete. In: Second RILEM International Conference on Concrete and Digital Fabrication – Digital Concrete 2020, RILEM Bookseries, 28. Springer, Cham, pp. 301–311. https://doi.org/10.1007/978-3-030-49916-7_31.

Markin, V., Krause, M., Otto, J., Schröfl, C., Mechtcherine, V., 2021. 3D-printing with foam concrete: from material design and testing to application and sustainability. J. Build. Eng. 43, 102870. https://doi.org/10.1016/j.jobe.2021.102870.

Muthukrishnan, S., Ramakrishnan, S., Sanjayan, J., 2021. Technologies for improving buildability in 3D concrete printing. Cement Concr. Compos. 122, 104144. https://doi.org/10.1016/j.cemconcomp.2021.104144.

Mydin, M.A.O., 2011. Effective thermal conductivity of foamcrete of different densities. Concr. Res. Lett. 2 (1), 181–189.

Mydin, M.A.O., 2022a. Influence of density, porosity and void size on thermal conductivity of green lightweight foamed concrete. J. Adv. Res. Fluid Mech. Therm. Sci. 92 (2), 25–35. https://doi.org/10.37934/arfmts.92.2.2535.

Mydin, M.A.O., 2022b. Investigating the effect of sisal fibre content on durability properties of lightweight foamed concrete. Adv. Sci. Technol. Res. J. 16 (2), 141–149. https://doi.org/10.12913/22998624/147065.

Nambiar, E.K.K., Ramamurthy, K., 2006. Influence of filler type on the properties of foam concrete. Cement Concr. Compos. 28 (5), 475–480. https://doi.org/10.1016/j.cemconcomp.2005.12.001.

Nambiar, E.K.K., Ramamurthy, K., 2007. Air-void characterisation of foam concrete. Cement Concr. Res. 37, 221–230. https://doi.org/10.1016/j.cemconres.2006.10.009.

Panesar, D.K., 2013. Cellular concrete properties and the effect of synthetic and protein foaming agents. Construct. Build. Mater. 44, 575–584. https://doi.org/10.1016/j.conbuildmat.2013.03.024.

Rahul, A.V., Santhanam, M., Meena, H., Ghani, Z., 2019. 3D printable concrete: mixture design and test methods. Cement Concr. Compos. 97, 13–23. https://doi.org/10.1016/j.cemconcomp.2018.12.014.

Raj, B., Sathyan, D., Madhavan, M.K., Raj, A., 2020. Mechanical and durability properties of hybrid fiber reinforced foam concrete. Construct. Build. Mater. 245, 118373. https://doi.org/10.1016/j.conbuildmat.2020.118373.

Ramamurthy, K., Kunhanandan Nambiar, E.K., Indu Siva Ranjani, G., 2009. A classification of studies on properties of foam concrete. Cement Concr. Compos. 31, 388–396. https://doi.org/10.1016/j.cemconcomp.2009.04.006.

Rollakanti, C.R., Prasad, C.V.S.R., 2022. Applications, performance, challenges and current progress of 3D concrete printing technologies as the future of sustainable construction – a state of the art review. Mater. Today Proc. https://doi.org/10.1016/j.matpr.2022.03.619.

Rudziewicz, M., Maroszek, M., Góra, M., Dziura, P., Mróz, K., Hager, I., Hebda, M., 2023. Feasibility review of aerated materials application in 3D Concrete Printing. Materials 16, 6032. https://doi.org/10.3390/ma16176032.

Sang, G., Zhu, Y., Yang, G., Zhang, H., 2015. Preparation and characterization of high porosity cement-based foam material. Construct. Build. Mater. 91, 133–137. https://doi.org/10.1016/j.conbuildmat.2015.05.032.

Schmid, R., Hansemann, G., Autischer, M., Juhart, J., 2022. Adaptive foam concrete in digital fabrication. In: Third RILEM International Conference on Concrete and Digital Fabrication – Digital Concrete 2022, RILEM Bookseries, 37. Springer, Cham, pp. 22–28. https://doi.org/10.1007/978-3-031-06116-5_4.

Song, Q., Bao, J., Xue, S., Zhang, P., Mu, S., 2021. Collaborative disposal of multisource solid waste: influence of an admixture on the properties, pore structure and durability of foam concrete. J. Mater. Res. Technol. 14, 1778–1790. https://doi.org/10.1016/j.jmrt.2021.07.075.

Tay, Y.W.D., Qian, Y., Tan, M.J., 2019. Printability region for 3D concrete printing using slump and slump flow test. Compos. Part B. 174, 106968. https://doi.org/10.1016/j.compositesb.2019.106968.

Van Der Putten, J., Rahul, A.V., De Schutter, G., Van Tittelboom, K., 2021. Development of 3D printable cementitious composites with the incorporation of polypropylene fibers. Materials 14, 4474. https://doi.org/10.3390/ma14164474.

Wu, P., Wang, J., Wang, X., 2016. A critical review of the use of 3-D printing in the construction industry. Autom. ConStruct. 68, 21–31. https://doi.org/10.1016/j.autcon.2016.04.005.

Xiao, J., Ji, G., Zhang, Y., Ma, G., Mechtcherine, V., Pan, J., Wang, L., Ding, T., Duan, Z., Du, S., 2021. Large-scale 3D printing concrete technology: current status and future opportunities. Cement Concr. Compos. 122, 104115. https://doi.org/10.1016/j.cemconcomp.2021.104115.

Zhang, N., Sanjayan, J., 2024. Quick nozzle mixing technology for 3D printing foam concrete. J. Build. Eng. 83, 108445. https://doi.org/10.1016/j.jobe.2024.108445.

Zhang, X., Li, M., Lim, J.H., Weng, Y., Tay, Y.W.D., Pham, H., Pham, Q.-C., 2018. Large-scale 3D printing by a team of mobile robots. Autom. ConStruct. 95, 98–106. https://doi.org/10.1016/j.autcon.2018.08.004.